PCCP

Superoctahedral two-dimensional metallic boron with peculiar magnetic properties

Journal:	*Physical Chemistry Chemical Physics*
Manuscript ID	CP-ART-07-2019-003786.R1
Article Type:	Paper
Date Submitted by the Author:	11-Aug-2019
Complete List of Authors:	Tkachenko, Nikolay; Utah State University, Department of Chemistry and Biochemistry Steglenko, Dmitriy; Southern Federal University, Institute of Physical and Organic Chemistry Fedik, Nikita; Utah State University, Chemistry and Biochemistry Boldyreva, Natalia ; Southern Federal University, Institute of Physical and Organic Chemistry Minyaev, Ruslan ; Southern Federal University, Institute of Physical and Organic Chemistry; Minkin, Vladimir; Institute of Physical and Organic Chemistry, Southern Federal University; Southern Scientific Center, Russian Academy of Sciences Boldyrev, Alexander; Utah State University, Department of Chemistry and Biochemistry

Superoctahedral two-dimensional metallic boron with peculiar magnetic properties

Nikolay V. Tkachenko,[a] Dmitriy Steglenko,[b] Nikita Fedik,[a,b] Natalia M. Boldyreva,[b] Ruslan M. Minyaev,[b] Vladimir I. Minkin[b] and Alexander I. Boldyrev[a,b]*

[a]*Department of Chemistry and Biochemistry, Utah State University, Logan, Utah 84322, United States*

[b]*Institute of Physical and Organic Chemistry, Southern Federal University, 194/2 Stachka Ave., 344090, Rostov-on-Don, Russian Federation*

KEYWORDS: ferromagnetic boron, two-dimensional ferromagnetism, SSAdNDP analysis

ABSTRACT: Among the diversity of new materials, two-dimensional crystal structures attract significant attention of the broad scientific community due to its promising applications in nanoscience. In this work, we predicted a novel two-dimensional ferromagnetic boron material, which has been exhaustively studied with the DFT methods. The relaxed structure of 2D-B_6 monolayer consists of slightly flattened octahedral units connected with the 2c-2e B-B σ-bonds. Calculated phonon spectrum and conducted *ab initio* molecular dynamics simulation revealed thermal and dynamical stability of the designed material. The calculation of mechanical properties indicated relatively high Young modulus of 149 N m^{-1}. Moreover, the electronic structure indicates the metallic nature of 2D-B_6 sheet whereas the magnetic moment per unit cell is found to be 1.59 μ_B. The magnetism in 2D-B_6 monolayer could be described by the presence of two unpaired delocalized bonding elements inside of every distorted octahedron. Interestingly,

the nature of the magnetism does not lie in the presence of half-occupied atomic orbitals, as it was shown for the previously studied magnetic materials based on the boron. We hope that our prediction will provide new promising ideas in the further fabrication of boron-based two-dimensional magnetic materials.

INTRODUCTION

The diversity of boron allotropes is fascinating. Having in its arsenal one-dimensional, two-dimensional, and three-dimensional structures, boron is one of the most prospective elements for material science. Wide range of structures such as nanowires, nanotubes, clusters, fullerenes, 2D sheets has been studied both theoretically and experimentally in recent years [1-22]. The unique electronic properties such as Dirac cones were found for several 2D boron allotropes [16,19]. An even hotter topic is the search for two-dimensional boron structures with magnetic properties due to its potential use in microelectronic and spintronic devices. Even though the design of two-dimensional ferromagnetic materials is extremely interesting and prospective topic, there are still few examples of theoretical [23-35] and experimental [36,37] reports. To the best of our knowledge, only one 2D material made of boron with magnetic properties has been predicted to the date [20]. However, it was shown that *M*-boron (a monolayer consisting of B_{20} polyhedrons) should be an antiferromagnetic material with the ferromagnetic surface ordering. Following the idea of constructing 2D materials from the polyhedrons, we decided to test a monolayer material constructed from boron octahedrons. The three-dimensional bulk materials with octahedral B_6 fragments were experimentally obtained previously. Such crystal structures always include a metal atom (Ca, La, etc.) [38,39] since two electrons should be added to obtain a stable *closo* B_6 structure according to Wade's rules [40,41]. However, in current work, we predicted a stable superoctahedral magnetic boron material, without the inclusion of any metal atoms. Therefore,

this material is the second example of the magnetic and the first example of ferromagnetic two-dimensional boron ever predicted.

COMPUTATIONAL METHODS

All calculations for the solid state systems were performed using the Vienna Ab initio Simulation Package [42] (VASP) code with PAW [43,44] pseudopotentials. The generalized gradient approximation (GGA) expressed by the PBE functional [45] was applied. For the structure relaxation, the large 700 eV energy cut off with convergence threshold 10^{-8} eV for total energy was employed. Brillouin zone has been sampled by the Monkhorst-Pack method [46] with an automatic generated 31×31×5 Γ-centered k-point grid. To eliminate the interaction between 2D-B_6 planes, the vacuum space was chosen to be 15 Å. The phonon dispersion was calculated via the Phonopy code [47] using 4×4×1 supercell and 7×7×1 k-mesh. For the more accurate calculation of the magnetism in a 2D-B_6 unit cell, the state-of-art hybrid functional of Heyd, Scuseria, and Ernzerhof (HSE06) [48, 49] was used. The energy cutoff for such calculations was set to 500 eV, the energy convergence criterion was set to 10^{-6} eV and 17×17×3 k-point grid. Band structure and DOS calculations for 2D-B_6 were performed at the PBE functional level with 800 eV energy cutoff. To explore the magnetic ordering within the 2D-B_6 surface, the optimization of 2×2×1 supercell in nonmagnetic (NM), antiferromagnetic (AFM), and ferromagnetic (FM) configurations was done.

To evaluate the thermal stability the *ab initio* Born-Oppenheimer molecular dynamics (BOMD) simulations for 4×4×1 supercell (96 atoms) were carried out. The time of the simulation was set to 5 ps with a time step of 1 fs. To calculate the molecular dynamics at 300 K, a longer time of 10 ps was set. Temperature control was performed using Nose-Hover method [50].

The solid-state adaptive natural density partitioning (SSAdNDP) [51] algorithm was used to analyze the bonding pattern of the 2D-B_6 structure. The SSAdNDP follows an idea of periodic NBO method, [52] and allows to obtain not only classical Lewis elements such as 1c-2e lone pairs and 2c-2e bonds but also delocalized bonding elements (nc-2e). A plane-wave calculation was performed using 400 eV energy cut off with convergence threshold 10^{-6} eV for total energy and k-points grid 31×31×7. Then, plane-wave density was projected into the cc-pVTZ [53] AO basis set. Previously, it was shown that the SSAdNDP is a powerful tool for analyzing chemical bonding in 2D materials. [54-65]. All optimized geometries and obtained bonding patterns were visualized by Vesta software [66].

The global minimum of a B_6H_4 cluster was found using Coalescence Kick algorithm [67]. Five thousand trial structures were generated and optimized at PBE0/3-21G level of theory [68,69] for both singlet and triplet states. All structures within 20 kcal/mol from global minimum (GM) were reoptimized at the PBE0/aug-cc-pVTZ level. The bonding pattern was obtained using the AdNDP algorithm [70] as implemented in the AdNDP 2.0 code [71]. All calculations for molecules were performed using Gaussian16 program [72]. All results of molecular calculations were visualized by ChemCraft 1.8 software.

RESULTS AND DISCUSSION

The optimized crystal structure of the 2D-B_6 monolayer belongs to $P_{4/mmm}$ crystallographic group. The unit cell consists of six boron atoms that ordered in a slightly flattened octahedron. For such a symmetric structure we can distinguish two types of equivalent boron atoms (Fig. 1b). The B_I-B_I, B_I-B_{II} and B_{II}-B_{II} lengths within the unit cell are 2.08 Å, 1.69 Å, and 1.89 Å, respectively. In turn, B_{II}-B_{II} length between two neighboring unit cells is 1.62 Å, which is the shortest distance within the whole structure. The nature of these geometric features

will be discussed below. As for the magnetic properties, we found both nonmagnetic (NM) and ferromagnetic (FM) configurations of the unit cell. Noteworthy, the FM state is lower in energy than the NM state by 43 meV/atom, therefore the former one represents energetically more stable state of 2D-B_6. However, from the structural point of view, these two configurations almost coincide. For a comparison, the lattice constants, total energy, and atomic positions are given in Table 1.

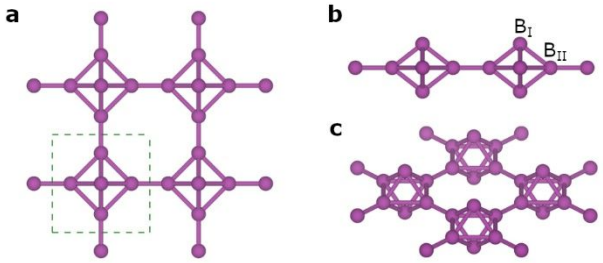

Figure 1. (a) The top view of the 2D-B_6 structure. The unit cell is shown with a green dashed square. (b) The side view of the 2D-B_6 structure. Two different types of boron atoms are labeled as B_I and B_{II}. (c) The angle view of the 2D-B_6 structure.

Table 1. Lattice constants, atomic positions and total energy of NM and FM 2D-B_6 monolayers.

Configuration	Type	Atomic positions	*a* (Å)	*b* (Å)	*c* (Å)	E_{tot} (eV/atom)
FM	B_I	(0.5, 0.5, 0.569) (0.5, 0.5, 0.431)	4.292	4.292	14.999	-5.762
	B_{II}	(0.189, 0.5, 0.5) (0.811, 0.5, 0.5) (0.5, 0.189, 0.5) (0.5, 0.811, 0.5)				
NM	B_I	(0.5, 0.5, 0.567) (0.5, 0.5, 0.433)	4.318	4.318	14.823	-5.719
	B_{II}	(0.190, 0.5, 0.5) (0.810, 0.5, 0.5) (0.5, 0.190, 0.5) (0.5, 0.810, 0.5)				

Since magnetic properties of the designed material are of our primary interest, we decided to study them at the more sophisticated level of theory. For the more accurate description of the magnetism, the HSE06 functional was used. The calculated magnetic moment per unit cell is found to be 1.59 μ_B. Noticeably, the magnetic moment is independent of the choice of density functional because almost the same results (1.56 μ_B) were obtained for PBE functional. The spin charge distribution for the FM 2D-B_6 sheet shows that spin density localized not only on the top and bottom boron atoms of the B_6 octahedron but delocalized through the structure (Fig.S1). That kind of delocalization might result in the partial 1.59 μ_B magnetic moment per unit cell. To confirm the magnetic surface state, 2×2×1 supercell of the 2D-B_6 sheet with different magnetic ordering was analyzed (Fig. 2). We found that the FM surface state is the most stable configuration, which is 0.10 and 1.02 eV/supercell lower in energy than AFM and NM states, respectively. Thereby, the 2D-B_6 is an exciting example of ferromagnetic material with ferromagnetic surface ordering.

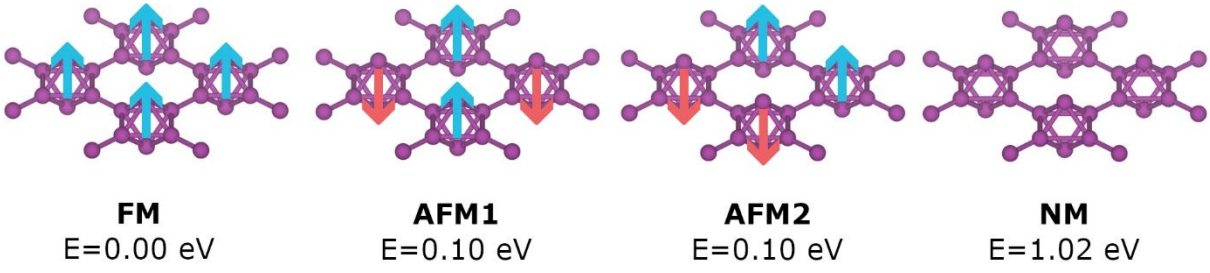

Figure 2. Magnetic ordering and relative total energies for 2×2×1 supercell of 2D-B_6 sheet.

The dynamic stability of the FM and NM configurations of 2D-B_6 was tested by calculating the phonon dispersion curves and phonon density of states. We showed that there are no low-lying dispersion curves entering the imaginary region in the whole Brillouin zone for the

ferromagnetic configuration (Fig. 3). The highest optical mode corresponds to in-plane vibrations and reaches ≈40 THz (1334 cm^{-1}) indicating the strong B-B interaction. Interestingly only ferromagnetic configuration is dynamically stable, while the nonmagnetic state has a large imaginary mode corresponding to the out-of-plane vibrations of B_{II} atoms (Fig. S2).

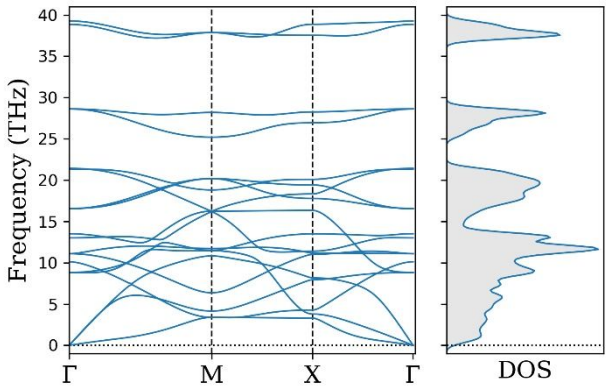

Figure 3. Calculated phonon dispersion curves along Γ-M-X-Γ path and phonon density of states for the ferromagnetic 2D-B_6.

In order to understand the electronic properties of the ferromagnetic 2D-B_6 material, we calculated an electronic band structure and a density of states (Fig. 4). We found that both spin up and spin down electrons have bands crossing the zero-energy level. As a result, 2D-B_6 has a nonzero density of states at the Femi level. These facts make the 2D-B6 sheet metallic without any band gap. For the comparison, the previously predicted *M*-boron is an AFM semiconductor with the indirect band gap 0.43 eV [20].

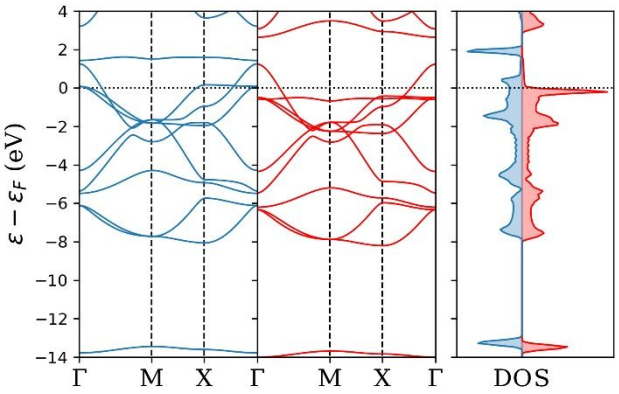

Figure 4. Calculated electronic band structure along Γ-M-X-Γ path and density of states for the ferromagnetic 2D-B_6. Red curves correspond to the spin up electrons, while the spin down electrons are illustrated with blue curves. The Fermi level is shown as a horizontal dotted black line.

The essential property of a material suitable for practical application is a thermal stability. We have performed spin-polarized *ab initio* Born-Oppenheimer molecular dynamics simulations at different temperatures (100 K, 300 K, and 450 K). The Nose-Hover thermostat was used for the temperature control. The time of simulation was set to 5 ps with a time step of 1 fs. For the 300 K simulation, longer time of 10 ps was chosen. A periodic 4×4×1 supercell (96 atoms) was used, large enough to demonstrate the structure and magnetic properties during the simulation. In Figure 5 fluctuations of the total magnetic moment and the temperature are shown as a function of the simulation time. An average total magnetic moment preserves remarkably large value at the end of simulations (25.4, 22.7 and 16.7 μ_B for 100, 300, and 450 K respectively). After 5 ps for 100 K and 10 ps for 300 K simulations, we found no significant structure distortion (Fig. S3). However, during the 450 K simulation, the structure was stable only for 3 ps. After that time, drastic structural deformations were observed. Thus, the 2D-B_6 structure is unstable at such a high temperature; octahedral fragments distorted severely transforming to the planar isomers

leading to a noticeable decrease in the magnetic moment of the material (Fig. 5). The root-mean square deviation from 0 K bond lengths is 0.07, 0.14, and 4.61 Å for 100, 300 and 450 K, respectively. As a result of these calculations, we can declare that the ferromagnetic 2D-B_6 monolayer survives at the temperatures up to 300 K, which opens a wide variety of potential applications. However, we should mention, that such temperature does not correspond to the Curie temperature, because the molecular dynamics simulation does not include spin dynamics. Obtained results indicate the stability of the magnetic state with respect to structural deformations.

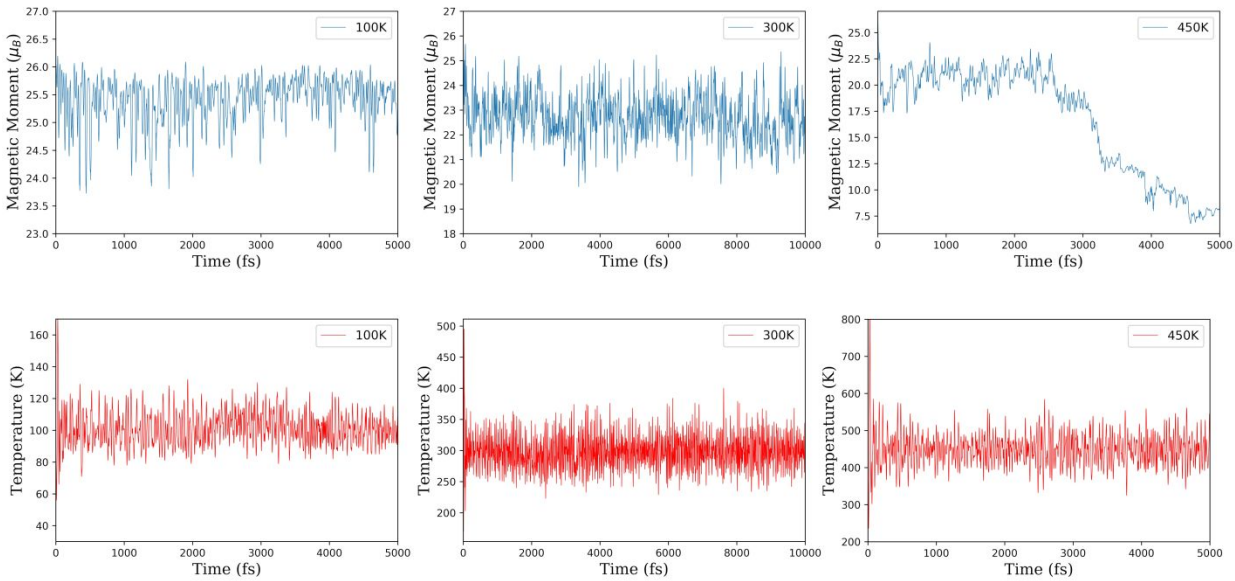

Figure 5. Calculated fluctuations of the total magnetic moment and temperature vs. simulation time step for 100 K (left column), 300 K (center column) and 450 K (right column).

Other important aspects of the promising material are the mechanical properties that characterize plasticity and elasticity of the material. The elastic constants, Young modulus, and Poisson's ratio for the 2D-B_6 monolayer are listed in the Table 2 (only two elastic constants

presented because the structure is isotropic). The Young modulus and Poisson's ratio were calculated according to the following formulas:

$$Y_{2D} = \frac{{c_{11}}^2 - {c_{12}}^2}{c_{11}} \quad \text{(I)}$$

$$\nu = \frac{c_{12}}{c_{11}} \quad \text{(II)}$$

Table 2. The calculated elastic constants (c_{ij}, in N m^{-1}), the Young modulus (Y_{2D}, in $N \cdot m^{-1}$), and Poisson's ratio (ν).

Structure	c_{11}	c_{12}	c_{66}	Y_{2D}	ν
2D-B_6	150.06	-12.59	9.84	149.01	-0.08

The question of how to synthesize this material remains to be open now. However, we hope that we are currently on the right track. Thus, studies on the preparation of singly charged compounds containing an octahedral B_6 fragment are underway [73]. We believe, that the results of these researches can be helpful for the synthesis of 2D-B_6.

To get insight into the chemical bonding of the 2D-B_6 monolayer we decided to analyze bonding pattern for a model D_{4h}-symmetric B_6H_4 cluster firstly. As for the spin state of the model cluster, we chose a triplet as the closest approximation to our ferromagnetic sheet. We should mention that the investigated structure has one imaginary frequency because it was forced to belong to D_{4h} symmetry. The gradient descends along the imaginary frequency led us to the less symmetric C_s structure. However, this distortion is not significant for the exploration of chemical bonding, and in the further discussion, the more symmetric structure will be considered for the convenience. The analysis of the potential energy surface *via* coalescence kick algorithm

reveals that the distorted octahedral geometry of B_6H_4 is 5.9 kcal/mol higher in energy than the planar global minimum structure (Fig. S6). However, the considered structure is still one of the lowest isomers for the chosen stoichiometry. In gas phase singlet state GM is more favorable than triplet GM by 9.3 kcal/mol. As for octahedral structures as building blocks for 2D-B_6 monolayer, singlet structure is lower in energy only by 1.4 kcal/mol. Obviously in crystal environment triplet state is stabilized since the calculated magnetic moment of unit cell clearly indicates the presence of unpaired electrons, therefore, bonding pattern for the triplet molecular cluster will be discussed.

The results of AdNDP analysis are presented in Figure 6. The bonding pattern can be described as four classical two-centered two-electron (2c-2e) B-H σ-bonds with occupation number (ON) 1.99 |e|, six 6c-2e bonds with ON = 2.00-1.96 |e|, and two unpaired alpha electrons which are forming 2c-1e B-B bond with ON = 0.98 |e| and 6c-1e bond with ON = 1.00 |e|. Unprecedently, 1e bonds are perpendicular to each other and we never observed such bonding feature before today.

Since it is not quite an intuitive result, we decided to build and evolution path of chemical bonding picture from the well known $B_6H_6^{2-}$ cluster to B_6H_4 species. The results could be found in the SI. The obtained bonding pattern for $B_6H_6^{2-}$ and $B_6H_4^{2-}$ as well as the comparison of MO energies pushed us to the conclusion that the presented bonding pattern is correct (Fig. S7-10). It is worth noting that we expected to find two 1c-1e bonds at the top and bottom apexes of B_6 unit (as it was observed, for previously predicted *M*-boron [20]). However, during the structure relaxation, we observed a change in the energy of molecular orbitals, which led to the formation of two one-electron bonds perpendicular to each other. These bonds provide a slightly flattened geometry for this cluster. We will see below that similar one-electron bonds were also found in

the 2D-B_6 monolayer. These bonding elements are responsible for the ferromagnetic properties of this material.

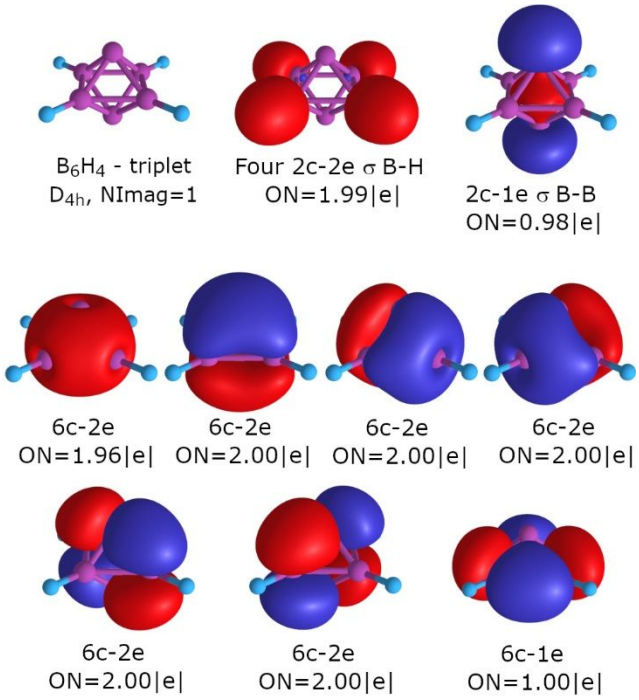

Figure 6. Overall chemical bonding picture obtained for the B_6H_4 cluster in the triplet state. The abbreviation ON denotes the occupation number of a certain bond.

To figure out the bonding picture in 2D-B_6 we used Solid State Adaptive Natural Density Partitioning (SSAdNDP) algorithm. Following the ideas extracted from the bonding of the B_6H_4 cluster, we obtained very cognate bonding pattern for the solid state. The results of SSAdNDP analysis for spin up and spin down electrons are presented in Figure 7. Each unit cell is bound with neighboring cells through the classical 2c-2e B-B σ-bonds with ON=1.93|e| (the equivalent of B-H σ-bonds for the cluster). The remaining electrons form eight delocalized six-centered one-electron bonds, which are responsible for binding interactions inside of each flattened

octahedron. For the spin up electrons we found a 6c-1e bond with ON = 0.99|e| (Fig. 7b) with the shape similar to the 2c-1e bond found in B_6H_4 cluster. Indeed, the contribution of two B_I atoms into the six-centered bond is found to be 97%. So, we can consider it as a pure 2c-1e bond. This chemical bond can cause the flattening of the B_6 octahedron. However, despite the chemical bonding for the cluster and solid state coincide for several bonding elements, we noted that the last three 6c-1e bonds of spin down electrons (Fig. 7o-q) behave differently. Instead of having one electron on each of the two 6c bonds (Fig. 7o, p), as it is observed in the case of B_6H_4, we have almost an equal low filling of three 6c bonds. The sum of the occupancies gives us about 2 electrons. Such an interesting behavior may be associated with a more explicit degeneration of these orbitals in the case of a solid state. Despite the described discrepancies in bonding patterns, the calculation of the difference between spin up and spin down occupancies provide us with the value 1.58 |e| which is in a very good agreement with calculated magnetic moment per unit cell (1.59 μ_B).

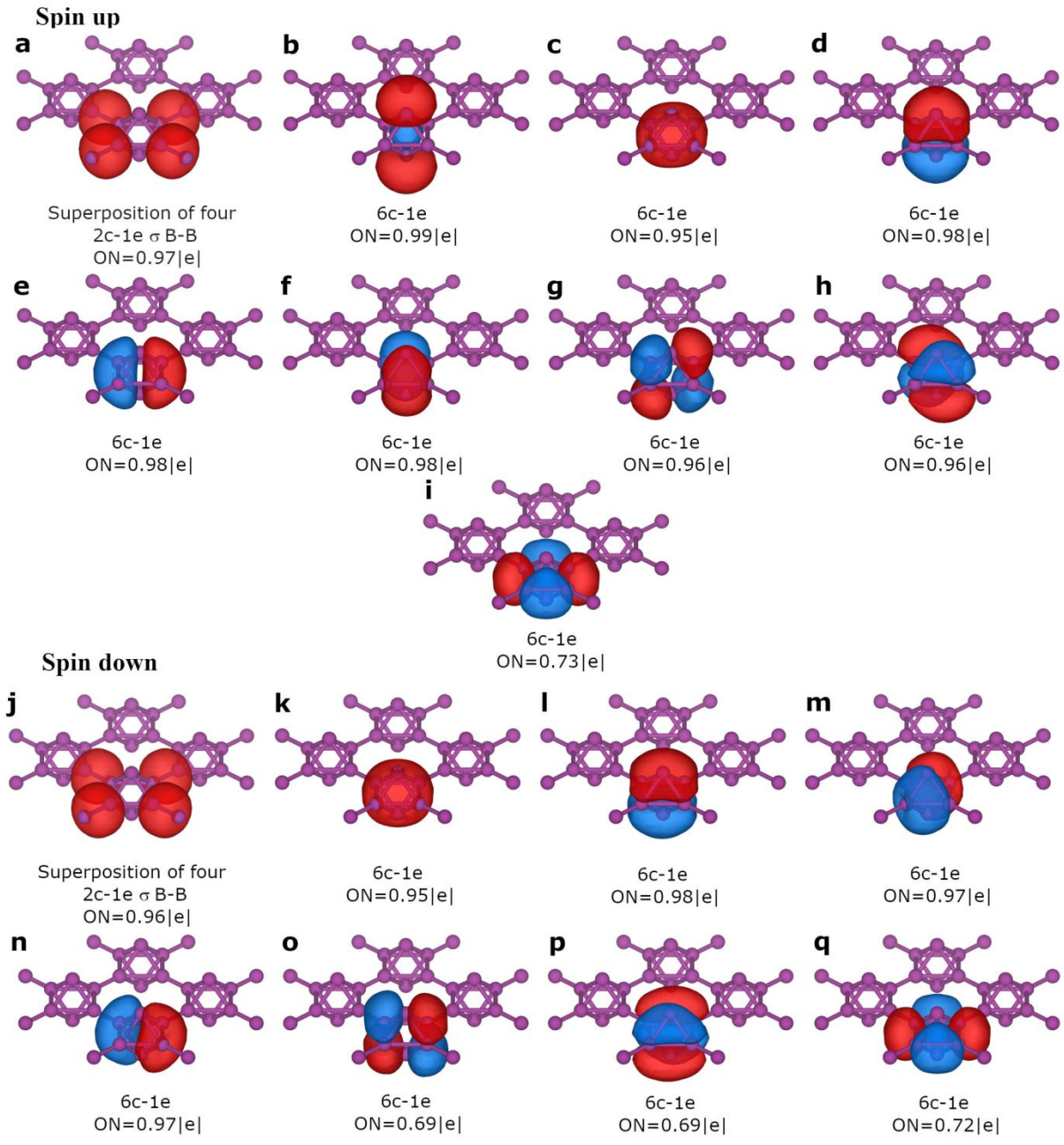

Figure 7. Overall chemical bonding picture obtained for the 2D-B_6 sheet. The results for spin up and spin down electrons are presented separately.

CONCLUISONS

To summarize, we designed and computationally tested a novel ferromagnetic superoctahedral 2D boron material. Based on the phonon spectrum and molecular dynamics simulation we managed to show that the 2D-B_6 monolayer is dynamically and thermally stable. Moreover, it has substantial magnetic properties and the calculated magnetic moment per unit cell is found to be 1.59 μ_B. The electronic structure indicates that this material is metallic, and its bonding pattern consists of classical 2c-2e bonds between unit cells and chemical bonding inside of the unit cell almost completely consists of six-centered bonds responsible for magnetic properties. To the best of our knowledge, the material designed in our work is the second example of magnetic 2D sheet and the first example of ferromagnetic metallic 2D sheet formed from pure boron. Therefore, we believe that this material is of great interest to modern material science and its thermal and mechanical stabilities promise a wide range of application once it is experimentally obtained.

ASSOCIATED CONTENT

Supporting information

The Supporting Information is available free of charge through the website ___.

Spin charge density distribution for the FM 2D-B_6; Calculated phonon dispersion and phonon density of states for the NM 2D-B_6; Final frames of each MD simulation test; Structures and relative energies of the lowest B_4H_6 isomers; Chemical bonding analysis of $B_6H_6^{2-}$, $B_6H_4^{2-}$ and B_6H_4 species.

AUTHOR INFORMATION

Corresponding Author

*E-mail: a.i.boldyrev@usu.edu.

ORCID

Alexander I. Boldyrev: 0000-0002-8277-3669

Author Contributions

The manuscript was written through contributions of all authors. All authors have given approval to the final version of the manuscript.

Notes

The authors declare no competing financial interest.

ACKNOWLEDGMENTS

The work was supported by the USA National Science Foundation (Grant CHE-1664379) to A.I.B.; D.S., R.M.M, V.I.M. and A.I.B. thank the Russian Ministry of Science and Education for the financial support. (Agreement No. 14.Y26.31.0016).

REFERENCES

(1) B. Albert and H. Hillebrecht, *Angew. Chem. Int. Ed.*, 2009, **48**, 8640.

(2) A. P. Sergeeva, I. A. Popov, Z. A. Piazza, W. L. Li, C. Romanescu, L. S. Wang and A. I. Boldyrev, *Acc. Chem. Res.*, 2014, **474**, 1349.

(3) H. J. Zhai, B. Kiran, J. Li and L. S. Wang, *Nat. Mater.*, 2003, **2**, 827.

(4) N. Gonzalez Szwacki, A. Sadrzadeh and B. I. Yakobson, *Phys.Rev. Lett.*, 2007, **98**, 166804.

(5) H. Tang and S. Ismail-Beigi, *Phys. Rev. Lett.*, 2007, **99**, 115501.

(6) D. L. V. K. Prasad and E. D. Jemmis, *Phys. Rev. Lett.*, 2008, **100**, 165504.

(7) H. Tang and S. Ismail-Beigi, *Phys. Rev. B*, 2009, **80**, 134113.

(8) S. Saxena and T. A. Tyson, *Phys. Rev. Lett.*, 2010, **104**, 245502.

(9) M. Liu, V. I. Artyukhov and B. I. Yakobson, *J. Am. Chem. Soc.*, 2017, **1395**, 2111.

(10) S. De, A. Willand, M. Amsler, P. Pochet, L. Genovese and S. Goedecker, *Phys. Rev. Lett.*, 2011, **106**, 225502.

(11) F. Liu, C. Shen, Z. Su, X. Ding, S. Deng, J. Chen, N. Xu and H. Gao, *J. Mater. Chem.*, 2010, **20**, 2197.

(12) E. S. Penev, S. Bhowmick, A. Sadrzadeh and B. I. Yakobson, *Nano Lett.*, 2012, **12**, 2441.

(13) X. Wu, J. Dai, Y. Zhao, Z. Zhuo, J. Yang and X. C. Zeng, *ACS Nano*, 2012, **6**, 7443.

(14) D. V. Steglenko, S. A. Zaytsev, R. M. Minyaev and V. I. Minkin, *Neorg. Khim.*, 2019, **64**, 1.

(15) H. Liu, J. Gao and J. Zhao, *Sci. Rep.*, 2013, **3**, 3238.

(16) X. F. Zhou, X. Dong, A. R. Oganov, Q. Zhu, Y. Tian and H. T. Wang, *Phys. Rev. Lett.*, 2014, **112**, 085502.

(17) X. F. Zhou, A. R. Oganov, X. Shao, Q. Zhu and H. T. Wang, *Phys. Rev. Lett.*, 2014, **113**, 176101.

(18) H. J. Zhai, Y. F. Zhao, W. L. Li, Q. Chen, H. Bai, H. S. Hu, Z. A. Piazza, W. J. Tian, H. G. Lu, Y. B. Wu, Y. W. Mu, G. F. Wei, Z. P. Liu, J. Li, S. D. Li and L. S. Wang, *Nat. Chem.*, 2014**, 6**, 727.

(19) M. Martinez-Canales, T. R. Galeev, A. I. Boldyrev and C. Pickard, *J. Phys. Rev. B*, 2017, **96**, 195442.

(20) X. F. Zhou, A. R. Oganov, Z. Wang, I. A. Popov, A. I. Boldyrev and H. T. Wang, *Phys. Rev. B*, 2016, **93**, 085406.

(21) Z. Zhang, E. S. Penev and B. I. Yakobson, *Chem. Soc. Rev.*, 2017, **46**, 6746.

(22) Z. Zhang, Y. Yang, E. S. Penev and B. I. Yakobson, *Adv. Funct. Mater.*, 2017, **27**, 1605059.

(23) J. Zhou and Q. Sun, *J. Am. Chem. Soc.*, 2011, **133**, 15113.

(24) Y. Liu, S. Bhowmick and B. I. Yakobson, *Nano Lett.*, 2011, **11**, 3113.

(25) Y. Ma, Y. Dai, M. Guo, C. Niu, Y. Zhu and B. Huang, *ACS Nano*, 2012, **6**, 1695.

(26) A. Du, S. Sanvito and S. C. Smith, *Phys. Rev. Lett.*, 2012, **108**, 197207.

(27) Z. Zhang, X. Zou, V. H. Crespi and B. I. Yakobson, *ACS Nano*, 2013, **7**, 10475.

(28) X. Li, X. Wu and J. Yang, *J. Am. Chem. Soc.*, 2014, **136**, 11065.

(29) F. Wu, C. Huang, H. Wu, C. Lee, K. Deng and E. Kan, *Nano Lett.*, 2015, **15**, 8277.

(30) Y. Wang, S. S. Wang, Y. Lu, J. Jiang and S. A. Yang, *Nano Lett.*, 2016, **16**, 4576.

(31) N. Miao, B. Xu, N. C. Bristowe, J. Zhou and Z. Sun, *J. Am. Chem. Soc.*, 2017, **139**, 11125.

(32) H. Kumar, N. C. Frey, L. Dong, B. Anasori, Y. Gogotsi and V. B. Shenoy, *ACS Nano*, 2017, **11**, 7648.

(33) Y. Sun, Z. Zhuo, X. Wu and J. Yang, *Nano Lett.*, 2017, **17**, 2771.

(34) Y. Zhao, J. J. Zhang, S. Yuan and Z. Chen, *Adv. Funct. Mater.*, 2019, **29**, 1901420.

(35) X. Zhou, X. Sun, Z. Zhang and W. Guo, *J. Mater. Chem. C*, 2018, **6**, 9675.

(36) C. Gong, L. Li, Z. Li, H. Ji, A. Stern, Y. Xia, T. Cao, W. Bao, C. Wang, Y. Wang, Z. Qiu, R. Cava, S. G. Louie, J. Xia and X. Zhang, *Nature*, 2017, **546**, 265.

(37) B. Huang, G. Clark, E. Navarro-Moratalla, D. R. Klein, R. Cheng, K. L. Seyler, D. Zhong, E. Schmidgall, M. A. McGuire, D. H. Cobden, W. Yao, D. Xiao, P. Jarillo-Herrero and X. Xu, *Nature*, 2017, **546**, 270.

(38) J. Akimitsu, K. Takenawa, K. Suzuki, H. Harima and Y. Kuramoto, *Science*, 2001, **293**, 1125.

(39) P. H. Schmidt, D. C. Joy, L. D. Longinotti, H. J. Leamy, S. D. Ferris and Z. Fisk, *Appl. Phys. Lett.*, 1976, **29**, 400.

(40) K. Wade, *Chem. Commun.*, 1971, **10**, 792.

(41) K. Wade, *Adv. Inorg. Chem. Radiochem.*, 1976, **18**, 1.

(42) G. Kresse and J. Hafner, *Phys. Rev. B*, 1993, **47**, 558.

(43) P. E. Blöchl, *Phys. Rev. B*, 1994, **50**, 17953.

(44) G. Kresse and D. Joubert, *Phys. Rev. B*, 1999, **59**, 1758.

(45) J. P. Perdew, K. Burke and M. Ernzerhof, *Phys. Rev. Lett.*, 1996, **77**, 3865.

(46) H. J. Monkhorst and J. D. Pack, *Phys. Rev. B*, 1976, **13**, 5188.

(47) A. Togo, F. Oba and I. Tanaka, *Phys. Rev. B*, 2008, **78**, 134106.

(48) J. Heyd, G. E. Scuseria and M. Ernzerhof, *J. Chem. Phys.*, 2003, **118**, 8207.

(49) J. Heyd, G. E. Scuseria, M. Ernzerhof, *J. Chem. Phys.*, 2006, **124**, 219906.

(50) G. J. Martyna, M. L. Klein and M. Tuckerman, *J. Chem. Phys.*, 1992, **97**, 2635.

(51) T. R. Galeev, B. D. Dunnington, J. R. Schmidt and A. I. Boldyrev, *Phys. Chem. Chem. Phys.*, 2013, **15**, 5022.

(52) B. D. Dunnington and J. R. Schmidt, *J. Chem. Theory Comput.*, 2012, **8**, 1902.

(53) T. H. Dunning, *J. Chem. Phys.*, 1989, **90**, 1007.

(54) A. S. Ivanov, E. Miller, A. I. Boldyrev, Y. Kameoka, T. Sato and K. Tanaka, *J. Phys. Chem. C*, 2015, **119**, 12008.

(55) H. Zhang, Y. Li, J. Hou, A. Du and Z. Chen, *Nano Lett.*, 2016, **16**, 6124.

(56) Z. H. Cui, E. Jimenez-Izal and A. N. Alexandrova, *J. Phys. Chem. Lett.*, 2017, **8**, 1224.

(57) C. Pu, D. Zhou, Y. Li, H. Liu, Z. Chen, Y. Wang and Y. Ma, *J. Phys. Chem. C*, 2017, **121**, 2669.

(58) Y. Wang, M. Qiao, Y. Li and Z. Chen, *Nanoscale Horiz.*, 2018, **3**, 327.

(59) I. A. Popov and A. I. Boldyrev, *J. Phys. Chem. C*, 2012, **116**, 3147.

(60) X. F. Zhou, A. R. Oganov, Z. Wang, I. A. Popov, A. I. Boldyrev and H. T. Wang, *Phys. Rev. B*, 2016, **93**, 085406.

(61) I. A. Popov, K. V. Bozhenko and A. I. Boldyrev, *Nano Res.*, 2012, **5**, 117.

(62) M. Martinez-Canales, T. R. Galeev, A. I. Boldyrev and C. J. Pickard, *Phys. Rev. B*, 2017, **96**, 195442.

(63) L. M. Yang, I. A. Popov, A. I. Boldyrev, T. Heine, T. Frauenheim and E. Ganz, *Phys. Chem. Chem. Phys.*, 2015, **17**, 17545.

(64) L. M. Yang, I. A. Popov, T. Frauenheim, A. I. Boldyrev, T. Heine, V. Bačić and E. Ganz, *Phys. Chem. Chem. Phys.*, 2015, **17**, 26043.

(65) L. M. Yang, V. Bačić, I. A. Popov, A. I. Boldyrev, T. Heine, T. Frauenheim and E. Ganz, *J. Am. Chem. Soc.*, 2015, **137**, 2757.

(66) K. Momma and F. Izumi, *J. Appl. Crystallogr.*, 2011, **44**, 1272.

(67) A. P. Sergeeva, B. B. Averkiev, H. J. Zhai, A. I. Boldyrev and L. S. Wang, *J. Chem. Phys.*, 2011, **134**, 224304.

(68) C. Adamo and V. Barone, *J. Chem. Phys.*, 1999, **110**, 6158.

(69) J. S. Binkley, J. A. People and W. J. Hehre, *J. Am. Chem. Soc.*, 1980, **102**, 939.

(70) D. Y. Zubarev and A. I. Boldyrev, *Phys. Chem. Chem. Phys.*, 2008, **10**, 5207.

(71) N. V. Tkachenko and A. I. Boldyrev, *Phys. Chem. Chem. Phys.*, 2019, **21**, 9590.

(72) M. J. Frisch, et al. *Gaussian 16*, Revision B.01 (Gaussian, Inc. 2016).

(73) X. Mu, J. C. Axtell, N. Bernier, K. Kirlikovali, D. Jung, A. Umanzor, K. Qian, X. Chen, K. Bay, M. Kirollos, A. L. Rheingold, K. N. Houk and A. Spokoyny, Preprint at ChemRxiv, 2019, https://doi.org/10.26434/chemrxiv.8097542.v1.